Infrared Spectrum of Matrix-Isolated CO and CO Photoproduct from OCS Photolysis†

David T. Anderson‡ and John S. Winn*

Department of Chemistry, Dartmouth College, Hanover, New Hampshire 03755

Received: September 2, 1999; In Final Form: February 9, 2000

Experimental studies on the photodissociation of OCS in both crystalline argon and nitrogen are presented. OCS photodissociation is followed by high-resolution interferometric infrared spectroscopy of the CO photoproduct. In solid nitrogen, the photogenerated CO molecule is produced in a damaged site that can be partially healed by thermal annealing. In contrast, the photogenerated CO site in argon does not revert to the sites occupied by neat CO/Ar matrices, even when annealed at 40 K. Model calculations on the infrared spectral line shape and orientational motion of the matrix-isolated CO molecule support a structural interpretation of the experimental findings. The calculations use an Ar−CO intermolecular potential along with an Ar_2 pair potential to minimize the energy of a finite section of the full matrix under two broad structural constraints and with both single- and double-substitutional site assumptions. The line shape is calculated via a CO center-of-mass motion weighted perturbation of the isolated CO intramolecular potential by the field of static Ar neighbors.

Introduction

The photodissociation of small molecules isolated in crystalline rare gas solids can serve as a simple prototype for condensed phase reaction dynamics. The structural simplicity of crystalline solids and the increasing availability of reliable intermolecular potentials for rare gas−molecule interactions offer unique advantages for a molecular understanding of condensed phase reactions, which are generally governed by the cage effect. The photodissociation dynamics of a variety of small molecule (HX, X_2, N_2O, H_2S, H_2O, CH_3X) rare gas systems have been studied both experimentally[1−6] and theoretically.[7−10]

Molecular dynamics simulations predict two general mechanisms that overcome the cage effect. If one photofragment has sufficient energy to exit the cage by a single direct collision, it will do so. This direct mechanism is quite different from the delayed exit mechanism, in which photofragments exchange energy with cage atoms more slowly before exiting or recombining. One mechanism usually dominates a system at any one photon energy. These simulations focus on events immediately after absorption of the dissociating photon, but another aspect of the cage effect is the long-term solvent relaxation around the nascent products.

High-resolution infrared spectroscopy in conjunction with an infrared spectral line shape theory provides a powerful method to study this latter aspect. The photofragment assumes the role of a probe chromophore that reflects its surroundings through its line shape. If this probe is also a stable molecule, it can be co-deposited with the same solvent and its line shape contrasted with the photofragment's.

A line shape theory that has successfully assigned solvent site geometries to the major infrared absorption features of OCS in Ar and Xe matrices is based on the perturbing influence of solvent packing on a solute normal mode.[11] Here, we use this theory to interpret the spectra of both the CO photofragment of OCS (which we will term photo-CO) as well as neat CO in N_2 and Ar matrices.

In the gas phase, OCS electronic absorption starts at 260 nm and reaches a maximum at 225 nm.[12,13] Photodissociation produces CO($X\ ^1\Sigma^+$) and either S(^{3}P) or S(^{1}D) which relaxes to ^{3}P.[14−18] The increase in the absorption coefficient with temperature has been used to support the assignment of the upper state geometry to a bent configuration.[19−22] This assignment agrees with model calculations based on a state-resolved study of the photofragment internal energy distribution.[18]

OCS photolysis in cryogenic solids has been used[23−26] to produce S and S_2 and as a convenient source of S atoms for subsequent reactions with O_2, NO, PX_3, and simple hydrocarbons.[27−29] The other photoproduct, CO($X\ ^1\Sigma^+$), has received little attention. The spectrum of *pure* matrix-isolated CO, however, has been extensively studied in rare gas solids[30−42] and in nitrogen.[43,44]

Experimental Section

The experimental method generally followed that of Lang and Winn.[45] Research grade (≥99.999%) matrix gases, OCS (97.7% purity, Matheson), and CO (Research grade, Linde) were used without further purification. Two deposition methods were employed. In one, 1250 Torr cm^3 amounts of a mixture were pulsed through a 0.53 cm inside diameter tube onto the matrix from a 10 cm^3 reservoir. Typically, 20 pulses were used to create the matrix. The other method deposited gas continuously from a 100 μm diameter molecular beam nozzle approximately 2 cm from the substrate. Typically, a backing pressure of 300 Torr was used for a 1 min deposition.

While the maximum experimental temperature is limited by the vapor pressure of the matrix gas, a layer of a less volatile substance deposited over an existing matrix can extend the experimental range. Thus, in some experiments, we coated Ar solvent matrices with 20 pulses of pure Xe at 20 K in order to extend the upper temperature range to ca. 40 K.

Spectra were recorded with a Bomem DA3.002 interferometric spectrometer at resolutions 0.005−0.1 cm^{-1} using a

† Part of the special issue "Marilyn Jacox Festschrift".

* To whom correspondence should be addressed. E-mail: jwinn@dartmouth.edu.

‡ Present address: Department of Chemistry, University of Pennsylvania, Philadelphia, PA 19104-6323.

10.1021/jp993126v CCC: $19.00
Published on Web 03/23/2000

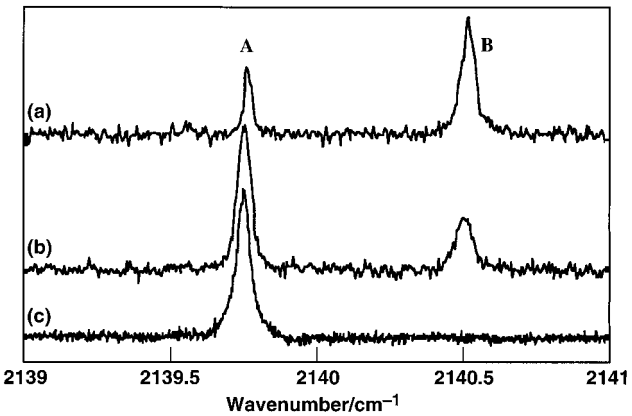

Figure 1. (a) 15 pulses (1500 cm^3 Torr) of OCS/N_2 = 1/5000 deposited and photolyzed for 4 h at 20 K, recorded at 12 K (0.01 cm^{-1} resolution). (b) After annealing (a) at 25 K; recorded at 12 K. (c) 2 min free jet deposition at 20 K of neat CO/N_2 = 1/100 000, recorded at 12 K (0.005 cm^{-1} resolution).

cooled InSb detector. Peak widths (full widths at half-maximum, fwhm) refer to absorbance measurements. Peak frequencies at any one matrix temperature are accurate to ≤0.004 cm^{-1} for the sharpest features as verified by calibration with gas phase spectra of OCS and H_2O.

The photolysis source was a 1000 W Hg/Xe high-pressure arc lamp, filtered by distilled water and focused on the sample. The sample was typically irradiated for 4 h at a temperature of 20 K.

Nitrogen Matrices. In N_2 matrices, pure CO exhibits a single sharp absorption at 2139.75 cm^{-1} at 12 K that red shifts 0.15 cm^{-1} as the temperature is raised to 30 K. Annealing the matrix at 25 K for 15 min immediately after deposition irreversibly decreases the CO line width slightly. The feature thereafter reversibly broadens (CO/N_2 = 10^{-5}, fwhm 0.03−0.06 cm^{-1}) over the 12−30 K range. The CO fwhm also decreases slightly as the CO concentration is decreased, reaching the limit stated here at approximately CO/N_2 = 10^{-5}. To compare with photolysis studies, CO mole fractions from 10^{-3} to 10^{-6} were studied. Narrowing after annealing at low concentrations and shifts with temperature agree with previous work.[43,44]

The spectrum of the ν_3 mode of OCS in N_2 is well-known.[45] The ^{32}S isotopomer's spectrum shows a sharp feature (0.051 cm^{-1} fwhm) at 2053.546 cm^{-1} at 20 K, and a broader (0.389 cm^{-1}) feature at 2056.18 cm^{-1} has been assigned[45] to a different site. After photolysis for 4 h, the OCS integrated absorbance is reduced by 48% for the main peak and 21% for the broad feature. This difference could indicate either interconversion between the two sites during irradiation and/or site-specific photodissociation efficiencies.

The frequency and line shape of the CO photofragment depend on the annealing history of the matrix and the photolysis temperature. Samples deposited and photolyzed at 20 K produced two features in the CO fundamental region: peak A at 2139.75 cm^{-1} (fwhm 0.04 cm^{-1}) and peak B at 2140.51 cm^{-1} (0.07 cm^{-1}) at 12 K. Photo-CO spectra before and after annealing at 25 K are compared to neat CO/N_2 in Figure 1. Peak A has the same position and line shape as freshly deposited CO/N_2 = 10^{-5}. Annealing at 25 K irreversibly increases the integrated absorption of peak A while diminishing peak B, but never totally removes it.

If the photolysis is carried out at 12 K instead of 20 K, the spectrum of photo-CO exhibits only peak B. This implies that the spectrum of photo-CO for photolysis at 20 K is the result of a sequence of two events. Initial photolysis produces CO in a damaged site (B) that can convert by thermal relaxation to a more stable site (A). Studies of the time dependence of this conversion showed that the intensity of peak A reaches a maximum and that of peak B falls to a minimum (about 40% of its initial value) during about 2 min annealing at 25 K. The spectrum is stable to further annealing at this temperature.

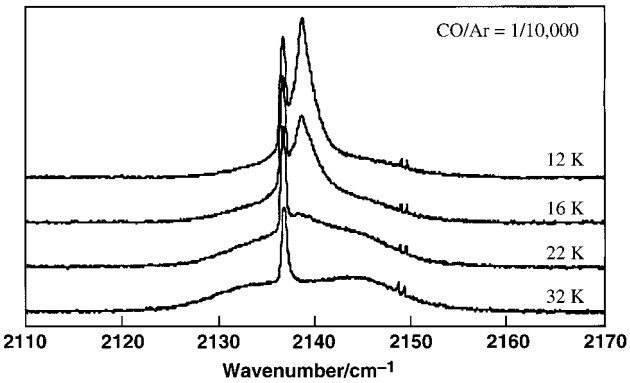

Figure 2. 8 min free jet deposit (400 Torr, 20 K) of neat CO/Ar = 1/10 000. The sample was annealed at 30 K for 15 min, and the spectrum was recorded at 12, 16, 22, and 32 K (0.01 cm^{-1} resolution).

Argon Matrices. Because the spectrum of CO in Ar is more complex than CO in N_2, it is important to establish this spectrum under a variety of conditions to be able to compare it with the spectrum of photo-CO. At high CO mole fractions (CO/Ar = 1/100), the major low-temperature peak at 2138.4 cm^{-1} has two satellite peaks at 2136.6 and 2140.0 cm^{-1}. Increasing temperature rapidly broadens the 2138.4 and 2140.0 cm^{-1} peaks while the peak at 2136.6 cm^{-1} broadens only slightly. The feature at 2140.0 cm^{-1} has been assigned to the CO dimer.[39] Peaks at 2148.8 and 2143.4 cm^{-1} that have been reported in other CO/Ar experimental work are absent from our spectra. These have been assigned to CO complexes with other impurities when slow spray-on deposition methods were used. Presumably, their absence is the result of our short deposition time. With either the pulse or molecular beam deposition methods, we were able to deposit a fresh matrix and record its spectrum in 15 to 30 min, under a dynamic vacuum on the order of 5 × 10^{-5} Torr, greatly reducing the chance of atmospheric background gas contamination.

At lower CO mole fractions, the relative absorbance of the peak at 2140.0 cm^{-1} is diminished, and the spectrum at 12 K is dominated by a broad feature (fwhm 1.4 cm^{-1}) at 2138.45 cm^{-1} with a sharper feature at 2136.6 cm^{-1}. Annealing enhances the red feature at the expense of the major feature. This reversible temperature broadening of the 2138.45 cm^{-1} peak is shown in Figure 2 for a CO/Ar = 1/10 000 sample. At 32 K, this peak is broadened over 20 cm^{-1} while the 2136.6 cm^{-1} peak has the same frequency and fwhm (0.78 cm^{-1}) as at 12 K. Repeated annealing at 40 K *did not* irreversibly deplete this peak, although it shifts from 2136.51 to 2136.66 cm^{-1} and broadens by 0.10 cm^{-1} over the 12−40 K range.

The spectrum of OCS/Ar before photolysis at 20 K agreed with earlier studies.[45] The ^{32}S isotopomer's main absorbance is a sharp feature (fwhm 0.051 cm^{-1}) at 2053.546 cm^{-1} (20 K), and a broad (0.389 cm^{-1}) feature at 2056.181 cm^{-1} has been assigned[11] to a different site. Photolysis was carried out until the OCS integrated absorbance dropped approximately 40%. After photolysis, a single sharp absorption appeared in the CO region at 2141.02 cm^{-1} (fwhm 0.09 cm^{-1}) that reversibly shifted 1.09 cm^{-1} to the red and broadened to 0.36 cm^{-1} when the temperature was increased from 12 to 40 K. Representative spectra of photo-CO at 12, 20, and 35 K are shown in Figure

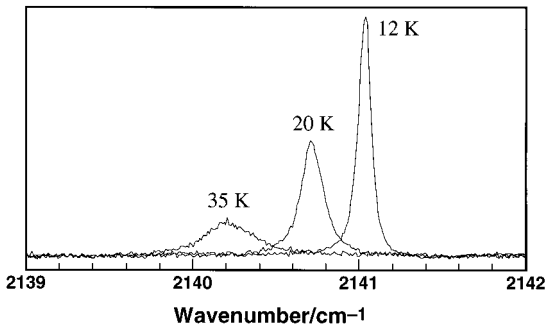

Figure 3. 20 pulses (1750 cm^3 Torr) of OCS/Ar = 1/4200 deposited at 20 K. After 6 h photolysis at 20 K, photo-CO spectra were recorded at 12, 20, and 35 K (0.02 cm^{-1} resolution).

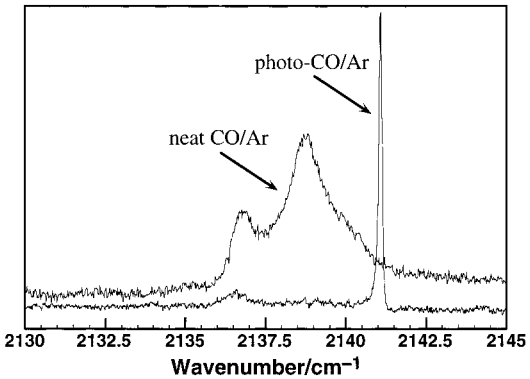

Figure 4. 20 pulses (1350 cm^3 Torr) of OCS/Ar = 1/4200 deposited at 20 K, photolyzed for 4 h, and cooled to 12 K, producing the photo-CO spectrum shown (0.02 cm^{-1} resolution). The neat CO/Ar spectrum is CO/Ar = 1/1000, deposited at 20 K, annealed at 35 K, and recorded at 12 K (0.01 cm^{-1} resolution).

3. In some of the spectra, there was a minor feature that was just discernible above the baseline to the red of the major photo-CO peak. A representative photo-CO spectrum where this feature is present is shown in Figure 4 along with a spectrum of neat CO. This minor feature matches the position, width, and temperature dependence the 2136 cm^{-1} feature of neat CO/Ar spectra. Annealing the matrix, even at 40 K, does not enhance this minor feature nor does it alter the photo-CO/Ar feature.

The photo-CO line shape is dramatically narrower than that of neat CO, as Figure 4 indicates. If the S(^{3}P) atom photofragment is responsible for this change, possibly any large inert atom introduced into the neat CO/Ar matrix will have a similar effect on the CO line shape. To test this possibility, samples of CO/Xe/Ar (1:10:1000) were deposited at 20 K, and a new feature was found at 2137.18 cm^{-1} between the two normal neat CO/Ar peaks as shown in Figure 5. Annealing the matrix at 35 K helps resolve the three peaks and increases the intensity of the 2136.6 cm^{-1} peak, just as in neat CO/Ar matrices. The new peak is narrower than the other two features and broadens slightly with an increase in temperature. CO/Xe matrices[46] have a strong absorption at 2133.5 cm^{-1}, but no feature at 2137 cm^{-1}. Therefore, the 2137.18 feature is most likely due to CO solvated by one or more Xe atoms, but not to CO totally solvated by Xe atoms. It is also considerably broader than and at a different frequency from the photo-CO peak.

Model Calculations

In order to understand the differences in line shapes and permanence of the photo-CO features in terms of the local structure of the matrix solvent surrounding OCS or CO, we have

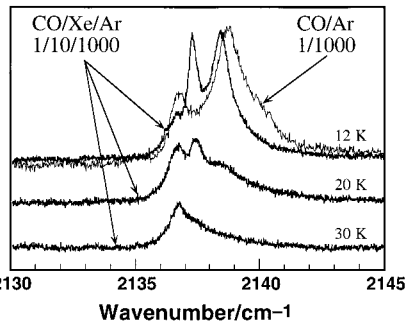

Figure 5. 20 pulses (1300 cm^3 Torr) CO/Xe/Ar = 1/10/1000 deposited at 20 K and recorded (0.01 cm^{-1} resolution) at 12, 20, and 30 K, compared to the neat CO/Ar spectrum of Figure 4 at 12 K.

TABLE 1: Equilibrium Distance, Angle, and Well Depth for the Two Ar−CO Potentials Used in This Work

Ar−CO potential form	R/Å	θ (deg)	$V_{XS}(R,\theta)$/cm^{-1}
Lennard-Jones (6-12)	3.543	70.2	−125.0
Buckingham (exp-6)	3.637	77.0	−110.4

applied a line shape theory described in ref 11 and a hindered rotation theory that was used to study HF and DF in Ar matrices in ref 47. Since the CO/N_2 intermolecular potential is not well-known, we have limited our calculations to the Ar matrix, and only details specific to the CO/Ar system are described here. Two important aspects, the choice of intermolecular potential and solvent configuration, are discussed in detail.

Highly accurate Dunham potential parameters represented the CO intramolecular potential.[48] For the weak bonds in the ArCO potential, we turn to spectroscopy of the ArCO van der Waals molecule for guidance. Both infrared and rotational spectra of the ArCO have recently been measured and characterized.[49] The molecule has a zero-point Ar to CO center of mass separation of 3.849 Å with a T-shaped geometry. Various ab initio and semiempirical potential energy surfaces have reproduced this T-shape with the Ar to CO center of mass vector making an angle around 80° ± 10° with the CO bond (with 0° representing a C−O−Ar linear configuration). Equilibrium well depths in the range 80−120 cm^{-1} are predicted. These surfaces have slight angular anisotropy and low barriers to motion of Ar around the CO along the minimum energy path. As a result, the van der Waals intermolecular vibrational modes are predicted to be those of a very loose complex with bends and stretches strongly coupled at energies approaching Ar−CO dissociation.

A Buckingham (exp-6) atom−atom ArCO intermolecular potential derived from solid-state data has been published by Mirsky.[50] We have used it and a Lennard-Jones (6-12) atom−atom potential with parameters taken from the original application of this theory to OCS/Ar. Table 1 presents the equilibrium distance, R, of Ar from the CO center of mass, the equilibrium angle θ between the vector from Ar to the CO center of mass and the vector from C to O, and the equilibrium well depth for these potentials with CO at its equilibrium bond length. An additional set of Lennard-Jones parameters was determined to reproduce R, θ, and the well depth predicted for Ar−CO from theoretical calculations on weakly bound complexes of CO by Parish et al.[51] The result was a potential where the Ar atom was closer to the oxygen end of CO (θ = 49°), R was larger (3.814 Å) and the well depth was larger (158 cm^{-1}). Calculation of the Ar−CO mixed second viral coefficient as a function of temperature for this potential significantly overestimated the experimental values (due to the large well depth), and no further calculations were carried out with it. The calculated line shapes for the exp-6 and first Lennard-Jones potentials were found to

be essentially equivalent so that only the exp-6 potential results are discussed here.

To model the matrix site, the solute (S) is substituted into an fcc lattice of solvent atoms (X). Temperature enters the calculation through the initial fcc lattice constant, chosen from known thermal expansion constants for Ar. To make the problem tractable, a finite region of the matrix is selected and the potential energy of this micromatrix is written as the sum over all the S−X and X−X interactions. The Ar−Ar interactions were assumed to follow a Lennard-Jones function using well-known[52] parameters ($R_{Ar-Ar} = 3.76$ Å; $D_{Ar-Ar} = 100$ cm^{-1}). The solvent configuration around the solute is determined by minimizing the potential energy of the system with a simulated annealing algorithm to which various physical constraints are applied.

This algorithm starts with an initial solvent configuration. Earlier studies[11] suggested that there are two important and obvious such configurations. The first, which we will call the crystal configuration, starts with the perfect crystal lattice positions for X in which one or more X atoms have been removed from the interior of the ensemble to create a cavity for S (and here there may be more than one choice of initial S position and/or orientation), and the ensemble is allowed to relax. In this configuration, S is surrounded by at least two nearest-neighbor shells of X atoms, and the outermost shell is constrained throughout the annealing to be fixed at its perfect crystal lattice configuration. The innermost shell (the nearest-neighbors to S) and S itself are allowed to move in order to minimize the ensemble energy, but the outermost shell provides an effective static potential field which mimics the eventual long-range crystal symmetry far from the solute defect site.

The second initial configuration of importance, called the cluster configuration, imagines that the entire matrix is made starting from S and then adding X atoms one at a time until the matrix is formed. In practice, this site is achieved by surrounding S with a single layer of nearest-neighbor X atoms, placed initially at their perfect lattice points, but allowed to move without any exterior constraint, as if an isolated X_nS cluster (where n is the nearest-neighbor number) was frozen into the matrix. To complete the line-shape calculation, additional X atoms are placed around the X_nS cluster as needed to simulate the full matrix. The number of additional X atoms needed will depend on the strength and range of the X−S potential, but generally only one or two additional layers are required.

It is not immediately obvious which type of substitution site, single or double, CO occupies in an argon matrix. Previously, CO has been assumed to occupy a single-substitution site. Here both single-substitution (SS) and double-substitution (DS) sites were explored. Thermodynamics can be used as a guide to identify which site is more stable, but the actual site adopted by a solute in a cryogenic matrix is controlled by a combination of thermodynamics and kinetics. The cooling process is rapid enough to trap defects into the lattice. Thus, the final solvation geometry around the solute may not be the absolute minimum energy configuration.

The single-substitution site ensemble consisted of 146 Ar atoms arranged in an fcc lattice of which a maximum of 54 were allowed to relax while maintaining an outer shell of fixed atoms. The double-substitution site consisted of 182 atoms of which as many as 72 were allowed to relax. It was found, however, that it was sufficient to relax the first and second nearest neighbors only.

Once a configuration is found through simulated annealing, the Ar atoms are held fixed throughout the remainder of the line-shape calculation. The center of mass of CO is translated along the CO bond direction inside the fixed Ar atom cavity, generating a potential energy function for CO motion in this cavity, as in a particle in a box problem. The one-dimensional Schrödinger equation for this motion is solved to find the zero-point energy and wave function. The wave function shows the degree to which CO is localized in the cavity, and, through its square, the probability of any one position. The CO is then placed at a series of positions spanning this wave function, and at each position, the C−O distance is scanned, keeping the center of mass fixed. At each C−O distance, the perturbation to the CO chemical bond potential function due to all the surrounding Ar atoms is calculated, and the CO vibrational Schrödinger equation is solved for this perturbed potential. In this way, the CO vibrational transition energy as a function of position in the cavity is calculated, and since the square of the center-of-mass translational wave function weights these positions, the line shape is simply the transition energy weighted by this function.

The perturbation to the CO bond potential is purely the mechanical Ar−C and Ar−O interaction; there is no assumption made about the overall effect (due to polarization or other effects) on the CO potential from the mean field of the Ar cavity. Consequently, the absolute matrix shifts of the CO transition from the gas phase are not reproduced well. Relative shifts from one type of site to another and the relative line shapes themselves, however, are expected to be reasonably accurate, as was shown earlier[11] in the OCS/Ar study. That study showed that the calculated spacing between the absorbance maxima of the two observed OCS/Ar sites, 2.05 cm^{-1}, was in good agreement with the experimental spacing, 1.90 cm^{-1}, although the absolute peak positions were calculated to be roughly 14 cm^{-1} above the observed positions. As long as the number of nearest neighbors around the CO is the same when one site is compared to another, the mean field approximation we make here that allows relative separations from one site's relaxed configuration line shape to be compared faithfully to that of a different configuration of the same type of site will have validity.

The same cavity potential can also be used to calculate angular eigenvalues and eigenfunctions for rotation of CO in the matrix site. The angular potential is written as an effective two-dimensional potential in the orientational angles θ and ϕ of CO about its center of mass. For computational purposes, this potential is fit to an expansion in terms of spherical harmonics, $Y_{l,m}$, of the form

$$V(\theta,\phi) = \sum_l a_1 Y_{l,0}(\theta,\phi) + \sum_{l,m} c_{l,m} Y^{C}_{l,0}(\theta,\phi) + d_{l,m} Y^{S}_{l,m}(\theta,\phi)$$

where the spherical harmonics are written as the real combinations

$$Y^{C}_{l,m} = \frac{(-1)^m Y_{1,m} + Y_{l,-m}}{\sqrt{2}}$$

$$Y^{S}_{l,m} = -\frac{i[(-1)^m Y_{l,m} - Y_{l,-m}]}{\sqrt{2}}$$

in which $e^{\pm im\phi}$ (with its phase factor) is replaced by $2^{1/2}\cos m\phi$ and $2^{1/2}\sin m\phi$, respectively. Fits included l,m values up to and including 9. The coefficients a_l, $c_{l,m}$, and $d_{l,m}$ in the expansion are determined by least-squares fits to the potential surface calculated by summing over all the Ar−CO interactions.

The angular wave functions $\Psi_i(\theta,\phi)$ are also expanded in spherical harmonics

$$\Psi_i(\theta,\phi) = \sum a_{i,j,k} Y_{j,k}(\theta,\phi)$$

so that matrix elements of the kinetic and potential energy operators are readily calculated. The eigenvalues and expansion coefficients are then found explicitly by matrix diagonalization. Calculations of angular energies were found to be converged to <0.1 cm^{-1} by $j, k \leq 15$.

Discussion

For the single-substitution crystal site, the energy required to create the vacancy is calculated to be 1631.57 cm^{-1} using the Ar−Ar pairwise potential. This compares favorably with the experimental sublimation energy and with other model calculations.[53] Annealing the matrix with CO in this vacancy produces subtle changes in this site. The first and second nearest-neighbor Ar atoms are displaced an average distance of 0.053 and 0.034 Å, respectively, from their fcc positions. The major effect of annealing was to relax the center of mass of CO approximately 0.25 Å from its original fcc position and orient it along a ⟨100⟩ crystal direction. The energy required to insert the CO molecule into the annealed Ar matrix is calculated to be 197 cm^{-1}. Thus, the annealed site is not thermodynamically costly, and the relaxation of the matrix around the CO molecule is minimal. These results are consistent with the modeling studies of Manz and Mirsky using the same Ar−CO potential function.[54]

For the cluster site, the average displacement of the first and second nearest-neighbor Ar atoms from their fcc positions increased to 0.17 and 0.13 Å, respectively, while the displacement of the center-of-mass of CO remained at 0.28 Å. Under this less constrained annealing condition the minimum energy configuration is further from the fcc lattice geometry than for the crystal annealed site. Obviously, the cluster annealed atoms move more than the crystal annealed case but the standard deviation also increases (from ±0.009 to ±0.04 Å). This is consistent with the concept of the cluster site being more amorphous near the solute.

Figure 6 shows the CO center-of-mass translational potentials, ground state wave functions, and lowest two translational energy levels for three of the four sites explored here. (The cluster annealed SS site is very similar to the crystal site shown here.) For the single-substitution sites, the potential is symmetric and nearly harmonic. Slices through the full potential surface in other directions are also closely harmonic. This symmetry reflects the high symmetry of the original octahedral lattice site and CO itself.

The cluster double-substitution site (the lowest panel in Figure 6) also shows CO localized to a small region of the cavity. In contrast, the crystal DS site (center panel) has a double-minimum potential, corresponding to either the C or the O atom of CO pointing toward the empty site. In the figure, the orientation, wave function, and local energy levels of the orientation with O pointing toward the empty site are shown. Hereafter, we will call this the "CO" orientation; the other orientation we will call "OC." The two configurations can interconvert by CO translation from one side to the other or by end-over-end rotation of CO in one side. They are separated by a potential barrier about 380 cm^{-1} high (the actual height depends on the simulation temperature), and they differ in well depth by less than 5 cm^{-1}, suggesting that they would be equally populated if present at all. For the OC orientation, the CO center of mass is located only 0.02 Å from the fcc lattice point, but for the CO orientation the center of mass has moved 0.55 Å toward the vacancy.

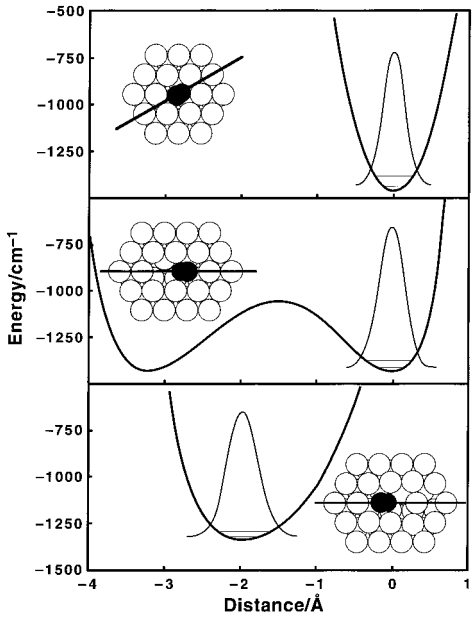

Figure 6. CO center-of-mass translational potentials, ground-state wave functions, and lowest two energy levels for translation along the CO bond direction for, top to bottom, the single-substitution crystal site, the double-substitution crystal site (with the orientation called "CO" in the text shown), and the double-substitution cluster site. The white circles represent the annealed locations of Ar atoms in each site's cutaway view.

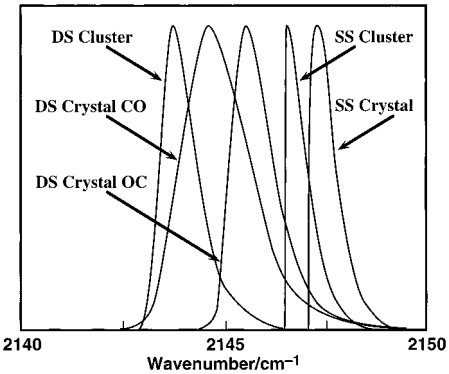

Figure 7. Calculated line shapes for the two types of single-substitution (SS) and three types of double-substitution sites.

The calculated line shapes for all five sites are shown in Figure 7. They all lie over a 3.5 cm^{-1} span. The transition center for the SS crystal site is 2147.29 cm^{-1} (fwhm 0.71 cm^{-1}) and 2146.58 cm^{-1} (fwhm 0.57 cm^{-1}) for the SS cluster site, a 0.71 cm^{-1} difference. For the ArCO van der Waals molecule, the fundamental transition is red-shifted by 0.4377 cm^{-1} from the monomer transition at 2143.2714 cm^{-1}.[49] The experimentally determined matrix shifts are −4.82 cm^{-1} for the strongly temperature-dependent peak and −6.61 cm^{-1} for the other peak. The calculations predict blue shifts primarily because no effects due to polarization of the CO bond by the matrix are taken into account, as mentioned earlier. Sevryuk and Billing[55] calculated the CO transition probabilities for the $0 \rightarrow 1$, $1 \rightarrow 0$, $1 \rightarrow 2$, $2 \rightarrow 1$, and $2 \rightarrow 3$ transitions for CO trapped in SS icosahedral sites of 12, 54, and 146 Ar atoms using a semiclassical simulation with a similar exp-6 potential, but they did not attempt a calculation of transition energies shifts. Similarly, Jansen's calculation[49n] of the ArCO van der Waals modes did

TABLE 2: Calculated Transition Centers, Fwhms, and $\Delta\nu_{matrix}$ for CO/Ar Sites

type of site	frequency (cm^{-1})	fwhm (cm^{-1})	$\Delta\nu_{matrix}$ (cm^{-1})
single substitution			
crystal	2147.29	0.71	4.02
cluster	2146.58	0.57	3.31
double substitution			
crystal OC	2145.55	1.15	2.28
crystal CO	2144.67	1.76	1.40
cluster	2143.80	0.95	0.53

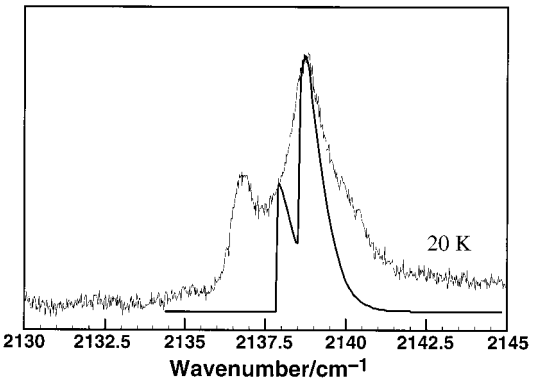

Figure 8. Comparison of the 20 K experimental CO/Ar spectrum (light line) with the calculated line shape based on single-substitution sites (heavy line).

not calculate the effect of complexation on the CO fundamental. This quantity, the absolute gas phase to matrix shift, remains a difficult quantity to calculate accurately for any solute. Consequently, we will concentrate on the relative frequency differences of our calculated line shapes and the detailed shapes themselves.

The energy required to insert CO into an annealed crystal double-substitution site (1754 cm^{-1}) is substantially larger than for a single-substitution site. Thus, while the transformation of a double-substitution site to a single-substitution site is thermodynamically favored, the conversion process is inherently a multibody process. The reorganizational barrier may be quite high (i.e., greater than 40 K) and kinetically unfavorable.

The cluster DS site is a result of this thermodynamic driving force toward a single-substitution site. The CO center of mass has moved 0.91 Å toward the center of the site, and the Ar atoms have relaxed substantially. The cluster site is much more amorphous with a larger average Ar atom displacement (0.39 Å) and greater amount of scatter in the displacements (±0.34 Å) than the crystal annealed sites (0.03 ± 0.01 Å). The line shapes for the two orientations of CO in the cluster DS site were found to be essentially equivalent. Thus, it is impossible to distinguish experimentally between the two, and only one configuration was used in subsequent calculations. The transition centers, fwhms, and $\Delta\nu_{matrix}$ for each site are summarized in Table 2.

Figure 8 compares the neat-CO/Ar spectrum at 20 K to the SS line shapes, shifted together and scaled so that the peak of the broader SS crystal line shape matches the broader experimental peak and the height of the SS cluster line shape matches the height of the experimentally narrower peak near 2136.6 cm^{-1} when the two calculated line shapes are added. Neither the widths nor the separation of the experimental peaks is well reproduced. Moreover, the calculated SS line shapes did not change width with matrix temperature in a way that could reproduce the experimental CO/Ar spectra as shown in Figure 2. In contrast, Figure 9 shows the experimental spectra at 12 and 20 K compared to the DS sites' calculated line shapes. In this figure, equal amounts of the CO and OC crystal sites' line shapes were added to the cluster site line shape, keeping all their calculated relative separations fixed and adjusting the crystal and cluster maxima to best reproduce the experimental spectra in a least-squares sense. These fits are much better, missing the observed splitting by less than 0.5 cm^{-1} and accurately reproducing the peak widths and overall shapes at both temperatures. There is a discernible shoulder in both spectra shown in Figure 9 to the red of the experimental main peak (near 2140.5 cm^{-1}) which is not reproduced by these DS fits. It is possible that the experimental intensity in the vicinity of 2140.5 cm^{-1} represents a minor contribution from a SS site (it is displaced about the right amount to the red to match our SS cluster calculated line), but the predominant conclusion from these spectra alone is that CO prefers a set of double-substitution sites in Ar matrices.

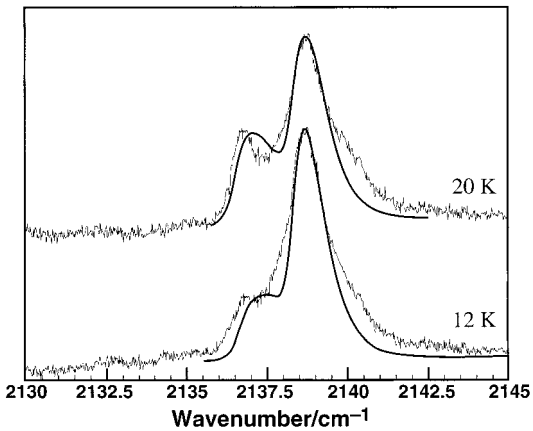

Figure 9. Comparison of 12 and 20 K experimental CO/Ar spectra (light lines) with calculated line shapes based on double-substitution sites (heavy lines).

The photo-CO spectra of Figures 3 and 4 are considerably narrower than any neat CO feature, as has been noted. Moreover, the photo-CO line shape is very symmetrical. Our narrowest calculated line shapes come from the SS sites, but they are broader and less symmetrical than the photo-CO spectra. The asymmetry of the calculated line shapes has an interesting origin. If the transition energy as a function of CO center-of-mass position has an extremum, the line shape will have a sharp falloff on one side or the other—to the red for the minima in these functions found here for the SS cluster site. Even a linear function need not lead to a symmetrical line shape if the ground state translational wave function is not symmetrical about its maximum. This is the case for the DS cluster site shown in the bottom panel of Figure 6 and accounts for the blue tail to the line shape shown in Figure 7.

The experimental spectra of CO/Xe/Ar mixtures in Figure 5 suggest that the presence of a large, inert, polarizable impurity atom in the Ar cage surrounding CO does not produce a CO line shape as narrow as the observed photo-CO spectra. This argues against a neighboring S(^{3}P) atom as the cause for the narrowing. Furthermore, the stability of the photo-CO line shape to high-temperature annealing, conditions under which it is known that S atoms diffuse, also argue against any role of S atoms in controlling the CO line shape. Moreover, since the S(^{3}P)−CO potential function is unknown, we did not attempt to model the CO line shape under conditions that would include a foreign cage atom.

Since a narrow line is, in this model, produced by at least one of the following conditions: a highly localized chromophore

or a chromophore only slightly perturbed by its neighbors, it seems likely that photolysis produces a cage that, while perhaps thermodynamically unstable and not discovered by an annealing simulation starting from a nearly thermodynamically stable configuration, is kinetically stable with an unusual structure.

Even though we do not reproduce the photo-CO spectrum from any site that is based on CO in a pure, relaxed Ar lattice, these simulations, the simulation of OCS in Ar, and the experimental behavior of the photo-CO spectra toward annealing lead to the following picture. Neat CO in Ar prefers double-substituted sites. One of these, the cluster site, is relatively stable toward annealing and leads to the 2136.6 cm^{-1} feature that does not change appreciably with temperature. The crystal sites, however, overlap and lead to the feature that broadens with temperature. Photolysis of OCS, however, must form CO in a single-substitution site, since OCS begins in a double-substitution site and the S atom photoproduct must either occupy the site adjacent to photo-CO (after relaxing to the inert $S(^3P)$ state) or exchange through diffusion with an Ar atom. The stability of the photo-CO spectrum to annealing implies that the initial site is stable, and the narrowness and temperature dependence of the spectrum implies a site that localizes CO to a high degree (as suggested by our SS cluster simulation, which produced the narrowest line shapes and the most localized site).

While the experimental spectra of neat and photo-CO show no evidence of hindered CO rotation, we have calculated the CO rotation (libration) energy levels for several types of sites to explore the degree to which low-lying librational states could be populated. The free CO rotational constant is small enough ($B_e = 1.9313$ cm^{-1}) that states might exist in unhindered sites that are within 30 cm^{-1} or so of the ground state. In fact, a librational level presumed to lie at ~11 cm^{-1} above the ground state has been invoked by Dubost[40] to explain a feature observed in his spectra, recorded at higher CO concentrations (CO/Ar = 1/1000) than ours. We see no such feature, and thus any calculated estimate of the excited translational or librational levels of CO has interest.

If the center of mass of CO is placed in a perfect fcc single-substitution site (of O_h symmetry), the molecule experiences an angular potential with 6-fold symmetry, a system first explored by Devonshire.[56] For our exp-6 potential, this O_h field has barriers from one minimum to the next of ~60 cm^{-1}, as shown in the contour plot of Figure 10a. In this potential, the $J = 1$ levels retain their degeneracy and lower their energy from the 3.85 cm^{-1} value of free CO to 1.76 cm^{-1}. The $J = 2$ levels split, with two falling from 11.54 to 2.91 cm^{-1} while the other three components rise to 24.74 cm^{-1}. Such a site would show the lowest hindered rotation levels thermally populated (or as vibration−rotation branches), but there is no evidence of such features.

Several variants of this site were explored. In one, the center of mass of CO was allowed to relax to its lowest energy position in the fcc SS site and the hindered rotation problem was solved for this configuration. Relaxation destroys the O_h symmetry, and the first excited level was found at 32.4 cm^{-1}. For the fully relaxed sites used in the line-shape calculations, the results were similar. Figure 10b−e plots the angular potential for these sites, and Figure 11 shows the lowest several energy levels for them in comparison to the free CO rotor levels. All relaxed sites show a first excited level more than 35 cm^{-1} above the ground state, indicating that libration excited states should not be thermally populated in neat CO/Ar matrices, as our spectra suggest, and indicating that the 11 cm^{-1} librational excited state hypothesized by Dubost is unlikely.

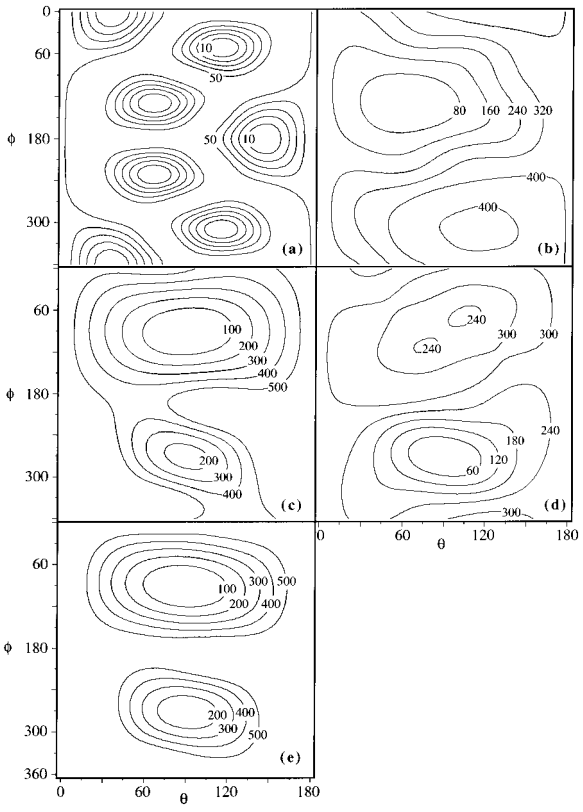

Figure 10. Potential energy contours for CO rotation in various sites. Energy values in cm^{-1} with respect to the minimum in each panel. (a) perfect fcc single-substitution site; (b) crystal single-substitution site; (c) CO crystal double-substitution site; (d) OC crystal double-substitution site; (e) cluster single-substitution site.

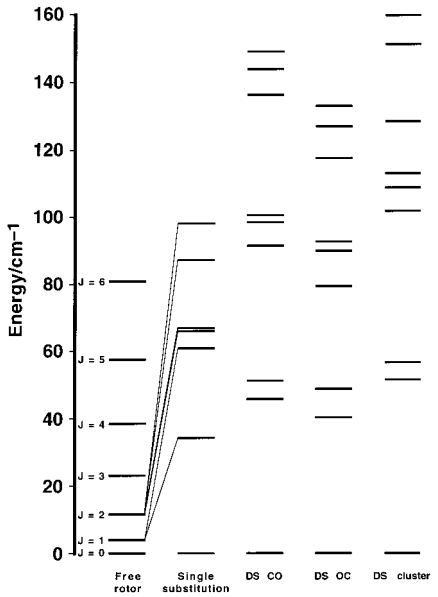

Figure 11. Rotation/libration energy levels for CO in various sites, compared to the gas-phase free-rotor levels of CO on the left.

Since these calculations were made for a fixed CO center of mass position in any one site, a few calculations were performed to explore at least qualitatively the effects of translation-rotation coupling. The extreme of such coupling assumes that the cage atoms follow the CO rotational motion and adiabatically lower the energy at each orientation. Model angular potentials were constructed under this assumption; at each CO orientation, the surrounding Ar cage and the CO center of mass were allowed

to move to establish a local potential minimum for the orientation. This angle-relaxed potential was then used in the hindered rotor calculation. In general, slightly lower energy levels were found, as relaxation lowers barriers in the angular potential, but since wells were also lowered and narrowed, the net effect was not dramatic.

The angle-relaxed potential for CO in a crystal single-substitution site had one interesting outcome, however. Relaxation of Ar around CO is minimal but enough to select a particular minimum energy CO orientation, and the hindered rotor calculations predicted the lowest two states to be very close in energy. Examination of the wave functions for these two states showed that both were predominantly $J = 0$ (s states), but they differed in CO orientation. These results are not realistic, because if the CO molecule flipped, the lattice would relax around the new orientation. Thus, allowing the center of mass to relax can provide insight into the coupling of translational and rotation, but the results must be analyzed critically.

Summary

Photolysis of OCS in N_2 matrices at 12 K produced a photo-CO molecule which was characterized by a sharp absorption feature that is shifted 0.75 cm^{-1} to the blue of the neat CO/N_2 absorption feature. This photo-CO feature can be largely, but not completely, converted to the neat CO/N_2 feature by annealing the matrix. This implies that at first the photo-CO molecule is produced in a metastable site.

The sharpness of the initial photo-CO feature suggests that while the site is metastable it is the same for all the photo-CO molecules. This supports the qualitative findings of other photodissociation studies that suggest a specific orientation of the chromophore (OCS) prior to absorption of the dissociating photon may have a much greater probability for subsequent dissociation. The long photolysis times (4 h) necessary to produce a sufficient number of dissociated photoproducts means that OCS absorbs enough energy to dissociate many times before it actually does. The matrix is very efficient at removing the excess dissociation energy from the absorbing molecule so that the majority of photodissociation events results in recombination. If the OCS molecule and its surrounding care are oriented in such a way that the photoproducts can exit the cage or if $S(^1D)$ relaxes quickly enough to ^3P, then the molecule dissociates and irreversibly forms photoproducts. Thus, even though a metastable geometry is initially produced, its geometry is consistent for the many successful photodissociation events so that instead of a broad transition or multiple peaks only one sharp photo-CO peak is produced.

The height of the reorganizational barrier between the two sites depends on the thermal history of the matrix. The barrier must depend not only on the local environment around the CO molecule but also on how the matrix atoms pack around the first solvation shell. Thus, the observed conversion rate reflects a distribution of individual barriers all with slightly different shapes. The experimental observation of an initial metastable photo-CO site is surprising given that photolysis can locally anneal the matrix. The many unsuccessful photodissociation events tend to soften the matrix around the absorbing molecule. This may further support the idea that the conversion process is a collective many-body process which necessitates that all the solvent molecules have sufficient thermal energy to surmount a cooperative barrier.

Photolysis of OCS in Ar matrices at 20 K produces a feature (2141.02 cm^{-1}, fwhm 0.09 cm^{-1}) that is considerably narrower and significantly shifted from the neat CO/Ar feature (2138.45 cm^{-1}, fwhm 1.4 cm^{-1}). Even high-temperature annealing at 40 K with a Xe overcoat is unable to convert the photo-CO/Ar feature to the neat CO/Ar feature. The 2.57 cm^{-1} separation between the photo and neat CO/Ar sites suggests the intermolecular cage forces on the photo-CO are unique. Such a large difference between the line shapes of the two features and the inability to thermally anneal the photo-CO site is surprising given that Ar is such a simple solid. Model calculations on the CO/Ar system support the hypothesis that OCS dissociation forms photo-CO in a single-substitution site quantitatively different from the double-substitution sites CO adopts when frozen in a CO/Ar mixture.

The orientational calculations predict that hindered rotation of neat CO/Ar should be quenched and the dominant orientational motion is libration. The dramatic reversible broadening of the CO 2138.4 cm^{-1} absorption feature is consistent with the population of excited translation−libration states of CO in DS sites that are not populated at lower temperatures. The librational calculations for crystal double-substitution sites predict that the first excited librational energy level is ~40 cm^{-1}, and the prediction of a barrier for translation of CO between the two double-substitution orientations suggests translation and libration may both contribute to the line broadening with an increase in temperature.

The other major neat CO/Ar feature, at 2136.6 cm^{-1}, is assigned to a cluster site that is a local minimum between a single-substitution and double-substitution site. This site is translationally localized, and the angular calculations predict librational levels above 50 cm^{-1}, consistent with a temperature-insensitive feature.

The OCS molecule before photolysis is known to be in a double-substitution site where rotation is quenched. It is localized on one side of the site, and the major degree of freedom is translational motion along the molecular axis. Photolysis can result in two basic geometries. In one, the CO and S atom photofragments are still present in the OCS cage but cannot recombine to form OCS because the S atom has relaxed to its ^3P ground state and/or the CO molecule has rotated to form CO···S. In the other, one of the photofragments has escaped from the OCS cage, and an Ar atom has moved into the other vacancy, effectively separating the two photofragments. Either scenario leaves photo-CO in a site that is basically a single-substitution site. This accounts for the experimentally determined blue shift of the photo-CO transition relative to the neat CO/Ar transition.

The model calculations predict that in Ar a single-substitution site is more stable than a double-substitution site. Neat CO/Ar must form only double-substitution sites for kinetic reasons. The CO molecule is not perfectly symmetric and is lighter than an Ar atom. Annealing the matrix helps the Ar atoms to try to squeeze into the additional vacancy, but they are not able to due to interactions among themselves as well as with the CO molecule. Similar studies on CO/Kr and CO/Xe matrices show a clear rare-gas size effect on the preferred matrix site.[46] It may also be that the photo-CO site is thermodynamically more stable than the neat CO/Ar site which is why no interconversion is measured even when the temperature of the matrix is raised to 40 K using a Xe overcoat.

Acknowledgment. This research was funded in part by a grant from the Petroleum Research Fund administered by the American Chemical Society. D.T.A. also thanks R. Ditchfield for many insightful discussions on the orientational calculations presented here.

References and Notes

(1) Bondybey, V. E.; Fletcher, C. J. *J. Chem. Phys.* **1976**, *64*, 3724.
(2) Becken, P.; Mendich, M.; Flynn, G. W. *J. Chem. Phys.* **1982**, *76*, 5995.
(3) Fajardo, M. E.; Apkarian, V. A. *J. Chem. Phys.* **1986**, *85*, 5660. Lawrence, W.; Okada, F.; Apkarian, V. A. *Chem. Phys. Lett.* **1988**, *150*, 339. Katz, A. I.; Apkarian, V. A. *J. Phys. Chem.* **1990**, *94*, 6671.
(4) Schriever, R.; Chergui, M.; Kunz, H.; Stepanenko, V.; Schwenter, N. *J. Chem. Phys.* **1989**, *91*, 4128. Schriever, R.; Chergui, M.; Unal, O.; Schwenter, N.; Stepanenko, V. *J. Chem. Phys.* **1990**, *93*, 3245. Schriever, R.; Chergui, M.; Schwenter, N. *J. Chem. Phys.* **1990**, *93*, 9206; **1991**, *95*, 6124.
(5) Feld, J.; Kunttu, H.; Apkarian, V. A. *J. Chem. Phys.* **1990**, *93*, 1009.
(6) Zoval, J.; Imre, D.; Ashjian, P.; Apkarian, V. A. *Chem. Phys. Lett.* **1992**, *197*, 549.
(7) Alimi, R.; Gerber, R. B.; Apkarian, V. A. *J. Chem. Phys.* **1988**, *89*, 14.
(8) Alimi, R.; Brokman, A.; Gerber, R. B. *J. Chem. Phys.* **1989**, *91*, 1611.
(9) Alimi, R.; Gerber, R. B. *Phys. Rev. Lett.* **1990**, *64*, 1453.
(10) Alimi, R.; Gerber, R. B.; McCaffrey, J. G.; Kunz, H.; Schwenter, N. *Phys. Rev. Lett.* **1992**, *69*, 856.
(11) Winn, J. S. *J. Chem. Phys.* **1991**, *94*, 5275.
(12) Okabe, H. *Photochemistry of Small Molecules*; Wiley-Interscience: New York, 1978; p 215.
(13) Breckenridge, W. H.; Taube, H. *J. Chem. Phys.* **1970**, *52*, 1713.
(14) Fournier, J.; Lalo, C.; Deson, J.; Vermeil, C. *J. Chem. Phys.* **1977**, *66*, 2556.
(15) Mankin, W. G.; Coffey, M. T.; Griffith, D. W. T.; Drayson, S. R. *Geophys. Res. Lett.* **1979**, *6*, 853.
(16) Sze, N. D.; Ko, M. K. W. *Atmos. Environ.* **1980**, *14*, 1223. Sze, N. D.; Ko, M. K. W. *Geophys. Res. Lett.* **1981**, *8*, 765.
(17) Rudolph, R. N.; Inn, E. C. Y. *J. Geophys. Res.* **1981**, *86*, 9891.
(18) Sivakumar, N.; Hall, G. E.; Houston, P. L.; Hepburn, J. W.; Burak, I. *J. Chem. Phys.* **1988**, *88*, 3692.
(19) Sidhu, K. S.; Csizmadia, I. G.; Strausz, O. P.; Gunning, H. E. *J. Am. Chem. Soc.* **1966**, *88*, 2412.
(20) Breckenridge, W. H.; Taube, H. *J. Chem. Phys.* **1970**, *53*, 1750.
(21) Ferro, B. M.; Reuben, B. G. *Faraday Soc. Trans.* **1971**, *67*, 2847.
(22) Jones, J. A. *J. Phys. Chem.* **1985**, *89*, 5366.
(23) Brom, Jr., J. M.; Lepak, E. J. *Chem. Phys. Lett.* **1976**, *41*, 185.
(24) Fournier, J.; Deson, J.; Lalo, C.; Vermeil, C. *Ber. Bungsenges. Phys. Chem.* **1978**, *82*, 100. Fournier, J.; Lalo, C.; Deson, J.; Vermeil, C. *J. Chem. Phys.* **1977**, *66*, 2556.
(25) Taylor, R. V.; Walker, W. C. *Appl. Phys. Lett.* **1979**, *35*, 359.
(26) Lee, Y.-P.; Pimentel, G. C. *J. Chem. Phys.* **1979**, *70*, 692.
(27) Long, S. R.; Pimentel, G. C. *J. Chem. Phys.* **1977**, *66*, 2219.
(28) Tso, T.-L.; Lee, E. K. C. *J. Phys. Chem.* **1984**, *88*, 2781.
(29) Hawkins, M.; Downs, A. J. *J. Phys. Chem.* **1984**, *88*, 1527, 3042. Hawkins, M.; Almond, M. J.; Downs, A. J. *J. Phys. Chem.* **1985**, *89*, 3326.
(30) Maki, A. G. *J. Chem. Phys.* **1961**, *35*, 931.
(31) Vu, H.; Atwood, M. R.; Vodar, B. *J. Chem. Phys.* **1963**, *38*, 2671.
(32) Abramowitz, S.; Broida, H. P. *J. Res. Natl. Bur. Stand.* **1964**, *68A*, 331.
(33) Leroi, G. E.; Ewing, G. E.; Pimentel, G. C. *J. Chem. Phys.* **1964**, *40*, 2298.
(34) Charles, S. W.; Lee, K. O. *Trans. Faraday Soc.* **1965**, *61*, 614.
(35) Barnes, A. J.; Hallam, H. E.; Scrimshaw, G. F. *Trans. Faraday Soc.* **1969**, *65*, 3172.
(36) Davies, J. B.; Hallam, H. E. *J. Chem. Soc., Faraday Trans. 2* **1972**, *68*, 509.
(37) Jiang, G. J.; Person, W. B.; Brown, K. G. *J. Chem. Phys.* **1975**, *62*, 1201.
(38) Dubost, H.; Abouaf-Marguin, L. *Chem. Phys. Lett.* **1972**, *17*, 269.
(39) Perutz, R. N.; Turner, J. J. *J. Chem. Soc., Faraday Trans. 2* **1973**, *69*, 452.
(40) Dubost, H. *Chem. Phys.* **1976**, *12*, 139.
(41) Dubost, H.; Lecuyer, A.; Charneau, R. *Chem Phys. Lett.* **1979**, *66*, 191.
(42) Swanson, B. I.; Jones, L. H. *J. Mol. Spectrosc.* **1981**, *89*, 566.
(43) Dubost, H.; Charneau, R.; Harig, M. *Chem. Phys.* **1982**, *69*, 389.
(44) Nelander, B. *J. Phys. Chem.* **1985**, *89*, 827.
(45) Lang, V. I.; Winn, J. S. *J. Chem. Phys.* **1991**, *94*, 5270.
(46) Hu, P.; Winn, J. S., unpublished results.
(47) Winn, J. S.; Anderson, D. T. *Chem. Phys.* **1994**, *189*, 171.
(48) Goble, Jr., J. H. Ph.D. Dissertation, University of California at Berkeley, 1982.
(49) Experiment: (a) De Piante, A.; Campbell, E. J.; Buelow, S. J. *Rev. Sci. Instrum.* **1994**, *60*, 858. (b) McKellar, A. R. W.; Zeng, Y. P.; Sharpe, S. W.; Wittig, C.; Beaudet, R. A. *J. Mol. Spectrosc.* **1992**, *153*, 475. (c) Havenith, M.; Hilpert, G.; Petri, M.; Urban, W. *Mol. Phys.* **1994**, *86*, 1003. (d) König, S.; Hilpert, G.; Havenith, M. *Mol. Phys.* **1995**, *86*, 1233. (e) Xu, Y.; Civis, S.; McKellar, A. R. W.; König, S.; Hilpert, G.; Havenith, M. *Mol. Phys.* **1996**, *87*, 1071. (f) Xu, Y.; McKellar, A. R. W. *Mol. Phys.* **1996**, *88*, 859. (g) König, S.; Havenith, M. *Mol. Phys.* **1997**, *91*, 265. (h) Ogata, T.; Jäger, W.; Ozier, I.; Gerry, M. C. L. *J. Chem. Phys.* **1993**, *98*, 9399. (i) Jäger, W.; Gerry, M. C. L. *J. Chem. Phys.* **1995**, *102*, 3587. (j) Hepp, M.; Jäger, W.; Pak, I.; Winnewisser, G. *J. Mol. Spectrosc.* **1996**, *176*, 58. (k) Hepp, M.; Gendriesch, R.; Pak, I.; Kuritsyn, Y. A.; Lewen, F.; Winnewisser, G.; Brookes, M. D.; McKellar, A. R. W.; Watson, J. K. G.; Amano, T. *Mol. Phys.* **1997**, *92*, 229. (l) Hepp, M.; Gendriesch, R.; Pak, I.; Lewen, F.; Winnewisser, G. *J. Mol. Spectrosc.* **1997**, *183*, 295. (m) McKellar, A. R. W. *Mol. Phys.* **2000**, *98*, 111. Theory: (n) Jansen, G. *J. Chem. Phys.* **1996**, *105*, 89 and references therein.
(50) Mirsky, K. *Chem. Phys.* **1980**, *46*, 445.
(51) Parish, C. A.; Augspurger, J. D.; Dykstra, C. E. *J. Phys. Chem.* **1992**, *96*, 2069.
(52) Winn, J. S. *Acc. Chem. Res.* **1981**, *14*, 341.
(53) Winter, M.; Seranski, K.; Schurath, U. *Chem. Phys.* **1992**, *159*, 235.
(54) Manz, J.; Mirsky, K. *Chem. Phys.* **1980**, *46*, 457.
(55) Sevryuk, M. B.; Billing, G. D. *Chem. Phys.* **1994**, *185*, 199.
(56) Devonshire, A. F. *Proc. R. Soc.* **1936**, *A153*, 601.
(57) These conclusions agree with those inferred in a report on new measurements of the CO/Ar spectrum that appeared after this paper was submitted: Abe, H.; Takeo, H.; Yamada, K. T. M. *Chem. Phys. Lett.* **1999**, *311*, 153.